RSC Chemical Biology

ROYAL SOCIETY OF CHEMISTRY

PAPER

View Article Online
View Journal

Cite this: DOI: 10.1039/d6cb00090h

Application of the YebF secretion pathway in *Escherichia coli* for rapid, on-plate screening of PETase libraries for improved activity

Jaeick Lee,*[a] Maame Yaa Yamoa,[a] Celina L. Bradley,[a] Graeme Howe *[ab] and David L. Zechel *[a]

Received 11th March 2026,
Accepted 19th May 2026

DOI: 10.1039/d6cb00090h

rsc.li/rsc-chembio

Plastic waste such as polyethylene terephthalate (PET) is a major environmental burden, and enzymes capable of degrading PET are emerging as biocatalytic tools for sustainable recycling. Progress in improving PET hydrolases (or PETases) has been constrained by the lack of simple and reliable screening systems. Here, we report a functional screen for PETase activity in *Escherichia coli* based on a zone-clearing assay, where the YebF secretory pathway is used to secrete YebF-PETase onto agar plates supplemented with bis(2-hydroxyethyl) terephthalate (BHET). Enzyme activity is observed as zones of clearance around *E. coli* colonies that express active YebF-PETases, as insoluble BHET is converted to soluble products. As proof of concept, the screen was used to evaluated libraries of YebF-leaf-branch compost cutinase (LCC) generated by site-saturation mutagenesis at the active site residues Y95, L102, and V212. This led to the identification of the more active LCC variants V212T and L102F–V212T. The secretion-based assay was then validated using turbidity assays and untagged LCC variants, where the L102F–V212T variant was confirmed to be more active against PET than the wild-type enzyme. Docking simulations indicated that V212T improves substrate positioning in the active site while L102F modifies surface charge and hydrophobicity, potentially enhancing binding to the hydrophobic substrate. Overall, the YebF secretion-driven functional screen serves as a straightforward platform for identifying improved PETase variants and potentially other plastic degrading enzymes.

Introduction

Plastics are an indispensable part of our day-to-day lives. Their durability, chemical inertness, high strength-to-weight ratios, affordability, and ease of production have led these materials to become ubiquitous in our society. Unfortunately, the durability and inertness of these materials has also led to the evolving plastic pollution crisis, wherein humanity's inability to recycle or otherwise degrade plastic wastes has led to massive, unchecked pollution of ecosystems around the globe. Current estimates suggest that approximately 300 million tonnes of plastic are produced each year,[1] and all available indications suggest that this quantity will continue increasing over the coming years.[2] Available recycling technologies are extremely limited, such that only ~10% of plastic waste is recycled.[3] Instead, most plastic waste is landfilled, incinerated, or otherwise mismanaged and released into the environment. Due to our inability to properly handle and dispose of this waste, living organisms across the globe are regularly exposed to macro-, micro-, and nanoplastics, and given the unclear effects of this exposure on the well-being of living organisms, plastic pollution represents both an ecological and a global health crisis.[1,4]

Biotechnological solutions to the plastic pollution crisis have been pursued for more than a decade, and significant progress has been made towards sustainable enzymatic recycling of polyethylene terephthalate (PET), a polyester with widespread utility in food packaging and textiles.[5,6] As of this writing, the Plastics-Active Enzymes Database (PAZy) lists 311 naturally occurring enzymes that degrade PET (''PETases''), suggesting that esterases capable of hydrolyzing the polyester backbone of PET are relatively common, especially when compared with hydrolytic enzymes active against polyamides (65 PAZy entries) and polyurethanes (39 entries).[7] While many naturally occurring PETases have been discovered and characterized, these enzymes are insufficient for large-scale PET recycling efforts, with limitations in activities, stabilities, and/or substrate inhibition patterns precluding their use in industrial recycling schemes. Directed evolution has been used to engineer PETase variants that overcome these limitations and

[a] Department of Chemistry, Queen's University, Kingston, ON, Canada. E-mail: gh80@queensu.ca, graeme.howe@queensu.ca, dlzechel@chem.queensu.ca
[b] Department of Biomedical & Molecular Sciences, Queen's University, Kingston, ON, Canada

maximize their utility as PET-recycling biocatalysts.[1,8–10] A particularly noteworthy PETase was engineered from a metagenome-derived cutinase discovered in composting leaves (LCC) and has enabled Carbios to pilot the biocatalytic recycling of 50 kilotons of PET waste per year at an industrial facility set to begin operations in 2026.[5,11] While natural PETases that are sufficiently efficient for large-scale recycling efforts might remain to be discovered, to date, directed evolution has been essential for the development of useful PETases.[9,12,13]

Given the importance of directed evolution for the development of efficient PET degrading enzymes, several methods have been developed to screen for PETase mutants with varying activities. Plate-based assays employing chromogenic PET-like molecules such as *p*-nitrophenyl esters have been developed, enabling rapid visual identification of variants with altered hydrolytic activity.[14] In addition, an ultrahigh-throughput yeast display platform was reported that allowed $>10^7$ mutant PETases to be screened for activity against cell surface-tethered substrate mimics.[15] While this method did lead to the identification of novel LCC variants that were more active against PET,[15] it is important to note that screening against substrate mimics may not always lead to improvements in hydrolytic activities against the authentic substrate of interest.[14]

This drawback is addressed by on-plate techniques that offer lower throughput but permit variant PETases to be tested for activity against the authentic plastic or components thereof. These assays generally use the size of zone of clearance ''halos'' that form as insoluble PET is digested into smaller oligomers as an indicator for PETase activity. Plate-based assays have been used to screen for PETase activity in the context of both enzyme discovery and engineering.[5,10,16,17] For example, halos observed when PET-doped agarose plates were treated with a library of >200 purified hydrolases derived from microbial genomes and environmental metagenomes led to the identification of ten novel PETases.[16] Directed evolution with on-plate assays generally involves transformation of a library of PETase variants into a heterologous expression host, followed by growth of the transformants on PET-doped agar. In these assays, each PETase must be released from the overexpressing colony for the enzyme to encounter the PET plastic in the surrounding media. Several methods have been explored to promote release of expressed PETases into the extracellular medium, including expression of PETases with secretion signal peptides in *E. coli*,[1,18,19] expression in alternative hosts (*i.e.*, *Pischia pastoris*) that promote export of heterologously overexpressed proteins,[20] and high-temperature or chemical lysis of cells.[10,21] Recent work has even shown that an engineered variant of LCC (''ICCG-LCC'') lacking any apparent signal peptide is naturally exported in *E. coli* to the extracellular space.[22] The natural secretion of this protein was exploited in a liquid culture-based assay that required several sub-culturing steps and the downstream chemical oxidation of terephthalic acid (TPA) released from PET into fluorescent 2-hydroxyterephthalate for detection.[23]

Here, we describe the first use of the YebF secretion signal to screen libraries of LCC mutants directly on agar plates. While the YebF tag was previously shown to enable rapid PETase screening in microplate format,[1] the on-plate assay described here permits sub-culturing steps to be bypassed, ultimately providing a faster, less resource-intensive screen for PETase activity that does not require cell lysis. The optimized screen permits differentiation of LCC variants based on activity while still maintaining the viability of the heterologous host colony. To demonstrate the utility of this method, libraries of LCC variants expressed in *E. coli* were screened on agar plates amended with bis(2-hydroxyethyl) terephthalate (BHET), an intermediate of PET hydrolysis, leading to the identification of previously unidentified variants that exhibit enhanced hydrolytic activity towards PET. In addition to the description of the novel screening methodology, this work presents validation of the identified mutations that conferred increased activity against PET through *in vitro* kinetic assays with purified mutants. Extensive *in silico* analysis was also undertaken, with the results of several docking studies suggesting that the identified mutations conferred enhanced activity against PET by subtly altering the active site cleft and the corresponding substrate binding modes.

Results and discussion

To explore the utility of protein secretion as an on-plate screening platform for plastic degrading enzymes, the YebF sequence from *E. coli* (GenBank ID: AAA23859.1) was fused directly to the *N*-terminus of LCC (XHB18896.1). We first examined the influence of the culture medium on the efficacy of the YebF tag to mediate extracellular secretion of active LCC from the bacterial cell. Autoinduction components were included in all media to simplify expression of the enzyme. Using *p*-nitrophenyl butyrate (*p*NPB) as a probe for esterase activity, the total hydrolytic activity was measured for supernatants of cultures grown in Luria-Bertani Broth (LB), Terrific Broth (TB), and Super Broth (SB) media (Fig. 1A). The total activity of the LB culture supernatant was 8.5 and 4.4 times higher than those observed with TB and SB, respectively. In contrast, the total hydrolytic activity of the soluble cellular fraction obtained from the TB and SB cultures were approximately equivalent, with both exhibiting about 1.6 times higher activities than the soluble cellular fraction obtained in LB. The hydrolytic activity of the supernatants relative to cell lysates was highest in LB, suggesting that LCC secretion levels were maximized in this media. This might suggest that media with fewer nutrients would favour YebF-mediated secretion by decreasing protein aggregation in the intracellular space and increasing efficiency of translocation across the *E. coli* membrane.[24,25] In contrast, the lower activities observed with the supernatants produced in TB and SB media might reflect a metabolic imbalance between protein synthesis necessary to support excessive proliferation and the Sec-dependent secretion of YebF.[24,26–28] Since the hydrolytic activity of the supernatant was maximized in LB, all subsequent

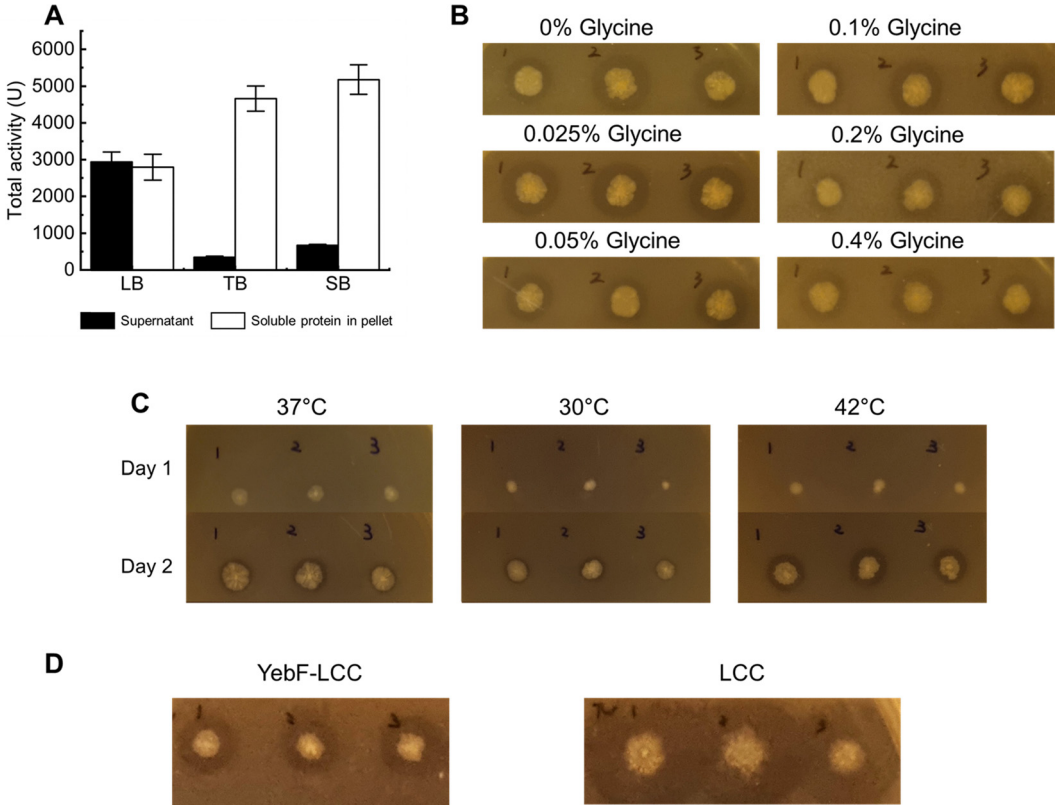

Fig. 1 Optimization of YebF mediated secretion of LCC from *E. coli*. (A) Assay of YebF-LCC esterase activity in the culture supernatant (total protein concentration 0.42–1.3 μM, 0.018–0.056 mg mL^{-1}) and soluble cytosolic fraction (1.0–2.0 μM, 0.043–0.086 mg mL^{-1}) of *E. coli* when grown in LB, TB, and SB auto-induction media (*p*NPB as substrate). (B) Effect of glycine concentration on the secretion of YebF-LCC from *E. coli* grown on LB agar plates containing 5 mM BHET (37 °C, 3 days). (C) Effect of temperature on YebF-LCC secretion from *E. coli* BL21 (DE3) grown on LB agar plates containing 5 mM BHET and 0.025% glycine at (i) 37 °C for 2 days, (ii) 30 °C for 2 days, or (iii) 30 °C for 1 day, then 42 °C for 1 day. (D) Comparison of clearance zone formation by YebF-LCC and LCC from *E. coli* BL21 (DE3) grown on LB agar plates containing 5 mM BHET and 0.025% glycine at 30 °C for 1 day followed by 42 °C for an additional day.

efforts to develop this secretion-based screen employed this media.

Next, we examined the ability of the YebF tag to secrete active LCC on solid media. In this assay, bis(2-hydroxyethyl) terephthalate (BHET) was used as the substrate. BHET is sparingly soluble in water and forms an opaque plaque when doped into LB agar plates.[3] BHET is also a direct intermediate produced during the enzymatic depolymerization of PET.[29–31] Therefore, we hypothesized that BHET would be a relevant substrate for initial screening of PETase activity, which could then be validated through enzymatic assays against polymeric PET. On an LB auto-induction agar plate containing 5 mM BHET, *E. coli* colonies harbouring the YebF-LCC expression construct failed to proliferate at 37 °C when inoculated *via* surface spreading (data not shown). In contrast, isolating a single colony from an LB agar plate and subsequently transferring it to an LB auto-induction agar plate supported robust growth. This inoculation strategy aligns with the use of auto-induction media or arabinose as an inducer as previously reported in the literature.[21,32] Following three days of incubation at 37 °C, *E. coli* colonies expressing YebF-LCC displayed distinct clearance zones (Fig. S1). This result suggested that the YebF tag successfully directed LCC into the extracellular space in an active form capable of hydrolyzing BHET into the more soluble products TPA and ethylene glycol (EG).

Previous studies had suggested that glycine could enhance protein secretion from *E. coli* by replacing L- and D-alanine in the peptidoglycan layer.[33–35] This supplementation results in the mild weakening of the *E. coli* cell wall and a corresponding increase in periplasmic leakage.[36] To examine the effect of glycine on the efficacy of the YebF-mediated secretion platform, *E. coli* colonies expressing YebF-LCC were grown on LB agar with varying glycine concentrations. The largest zones of clearance (relative to colony size) were observed when the LB agar plates contained 0.025% glycine (Fig. 1B). The effect of incubation temperature on the observed clearance was also evaluated, with the size of both the clearance zone and the transformants being larger at 37 °C. The incubation period could also be reduced significantly by first incubating the plates for one day at 30 °C before transferring the plates to a 42 °C incubator for an additional 24 h (Fig. 1C). As reported by others, the activity of the secreted LCC is enhanced at this increased temperature,[4,11,12] leading to larger clearance zones that could be easily and reliably quantified using ImageJ following the

two-day incubation. Using optimized media conditions, zone of clearances were also examined around colonies expressing the YebF-free PETase. In contrast to YebF-LCC, colonies expressing LCC produced much larger zones of clearance and appeared to undergo cell lysis (Fig. 1D and Fig. S8). This is consistent with the previous report of the ICCG-LCC variant undergoing secretion from *E. coli* despite lacking a secretion tag.[22] However, unlike LCC alone, YebF-LCC produced more consistent zones of clearance and colony dimensions, parameters that are necessary to accurately quantify enzyme activity.

Having established a protocol for the on-plate screening, the YebF-mediated zone-clearance assay was used to identify more active variants of LCC. A total of ten residues in or near the active site of LCC were identified using Hotspot Wizard as ones that could be mutated without deleterious effects on function (Fig. S2). At each position, the variant predicted to have the highest probability of preserving function was analyzed using induced fit docking simulations to predict binding affinities to dimeric or trimeric PET. GlideScores derived from these simulations, often used as indicators of binding affinities,[37,38] were then used to prioritize positions for site-saturation mutagenesis. These results suggested that LCC Y95F would bind the PET trimer with greater affinity than the wild-type (WT) enzyme, whereas LCC V212I was predicted to have enhanced affinity for the PET dimer (Fig. S3). In contrast, LCC L102I was predicted to bind both the dimer and trimer of PET more tightly than the WT. Interestingly, previous studies observed that substitution of a negatively charged residue in the equivalent position of LCC from *Ideonella sakaiensis* PETase (*Is*PETase) resulted in a small increase in activity.[39,40]

To demonstrate the utility of the YebF-based secretion assay to identify more active enzymes, we screened a limited number of LCC variants derived from site-saturated mutagenesis. Based on the suggested improvements in affinity for different oligomers of PET, Y95, L102, and V212 were separately subjected to site-saturation mutagenesis using degenerate primers. The plasmid pools encoding YebF-LCC Y95X, L102X, and V212X were individually transformed into *E. coli* BL21 (DE3) cells and cultivated on LB agar plates containing 0.025% glycine and 5 mM BHET (Fig. 2 and 3, Fig. S4 and S5). Gratifyingly, clearance zone sizes varied around each colony, potentially reflecting differences in the activities of the secreted PETase variants. To normalize this data, the area of each clearance zone and the corresponding colony was measured in ImageJ, with the ratio of these values being used as a normalized indicator of PETase activity. Four of the 31 colonies (#1, #3, #5 and #7) sampled in the V212X library displayed significantly higher clearance zone ratios than colonies expressing the WT enzyme (Fig. 2A and Fig. S4A). To confirm that this increase was statistically significant, two colonies (#5 and #7) were selected, grown in liquid LB media, then aliquoted in triplicate onto fresh LB agar plates with 0.025% glycine and 5 mM BHET. Following cultivation, greater clearance zone/colony ratios were observed once again for each replicate (relative to the WT), further indicating that these clones were overexpressing and secreting more active variants of LCC (Fig. 2B and Fig. S4B). While differences in halo size could also arise from differences in expression and secretion between variants, we show below that the activities of the purified enzymes correlate with halo size. Following plasmid purification and sequencing, clones #5 and #7 were found to harbour the V212T mutation. In the WT LCC, V212 appears to play a critical role in substrate binding through hydrophobic interactions within the active site. Therefore, substitutions at this position are likely to alter esterase activity, with V212T showing the highest BHET-degrading activity. Notably, this result is consistent with previous studies

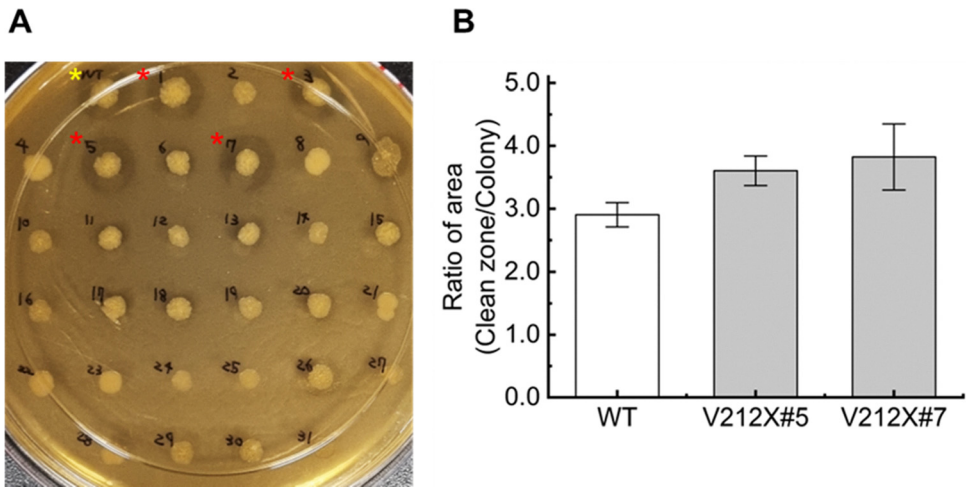

Fig. 2 Screening YebF-LCC V212X variants using a BHET zone clearing assay. (A) *E. coli* colonies expressing YebF-LCC-V212X variants were incubated on LB auto-induction agar plates supplemented with 0.025% glycine and 5 mM BHET. The plates were incubated at 37 °C for one day, followed by 42 °C for one day. The areas of the clearance zones and the corresponding colonies were measured with ImageJ and expressed as ratios (Fig. S4A). Colonies with zone of clearance: colony size ratios that are greater than that of the wild type (WT) YebF-LCC control (yellow asterisk) is marked with a red asterisk. (B) Selected *E. coli* colonies expressing more active V212X variants were used to inoculate LB-agar-BHET plates. Zone clearance ratios were measured in triplicate (Fig. S4B). Sequence analysis identified V212X#5 and V212X#7 as variants containing the V212T mutation.

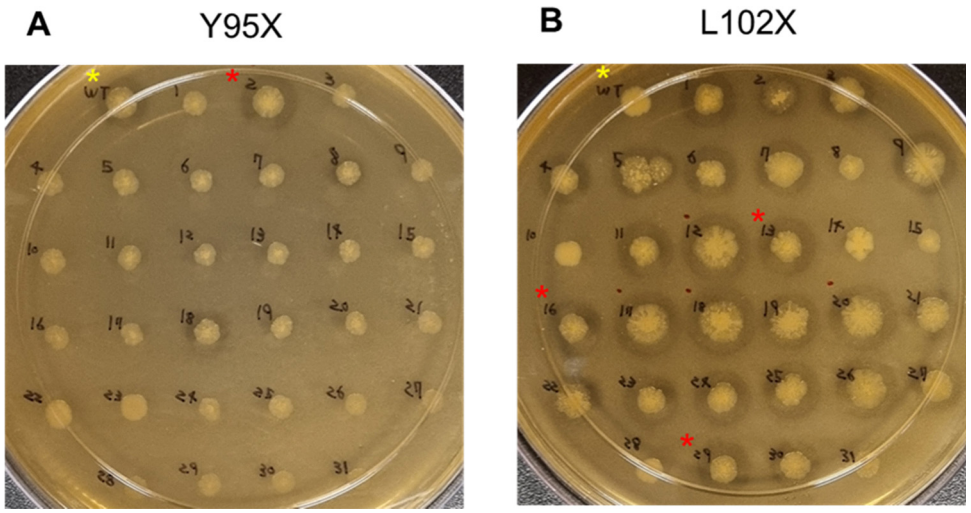

Fig. 3 Screening YebF-LCC-Y95X and L102X variants using a BHET zone clearing assay. Shown are colonies expressing YebF-LCC single-site variants derived from site-saturated mutagenesis of residues Y95 (A) and L102 (B). *E. coli* colonies expressing the variants were incubated on LB auto-induction agar plates supplemented with 0.025% glycine and 5 mM BHET. The plates were incubated at 30 °C for one day, followed by 42 °C for one day. The areas of the clearance zones and the corresponding colonies were measured using ImageJ and expressed as ratios (Fig. S5). Colonies expressing variants more active than wild-type (WT) YebF-LCC (yellow asterisk) are marked with a red asterisk.

reporting improved activity toward PET nanoparticles conferred by the same substitution,[41] and further validates the utility of the YebF-secretion screen.

The Y95X library was notable for producing few active variants. Only 6 of 62 colonies (#2, #18, #34, #42, #43 and #47) developed clearance zones, and these were equivalent to those observed with the WT enzyme (Fig. 3A and Fig. S5A and B). The active site residue Y95 is likely to provide a critical role for catalysis by LCC,[6,13,42] where the backbone amide of Y95 has been suggested to make up part of the oxyanion hole.[43] Although more colonies would need to be screened to assure that all 20 amino acids are sampled at this position, the low occurrence of active colonies in this small library suggests that only a limited number of substitutions are tolerated. Sequencing of the most active clone #42 revealed a Y95F variant of YebF-LCC (Fig. S6). Interestingly, several characterized PETases harbour Phe at the equivalent position of Y95.[44–46]

The LCC residue L102 resides on a hydrophobic face of an α-helix that is positioned near the active site cleft containing the catalytic triad. Substitutions at position L102 of LCC were significantly more permissive, with 23 of the 31 colonies overexpressing YebF-LCC L102X developing clearance zones. Several colonies gave rise to clearance zone ratios that were similar to those observed with colonies expressing WT YebF-LCC, while 3 colonies (#13, #16 and #29) gave clearance ratios greater than WT (Fig. 3B and Fig. S5C). Rather than sequencing active clones at this stage, and due to the frequent occurrence of active colonies in the L102X library, we hypothesized that screening L102X variants in the presence of the previously identified V212T substitution would lead to more active double-variants. Accordingly, 15 colonies overexpressing the V212T-L102X variants of YebF-LCC were screened using the secretion assay, and seven colonies (#1, #2, #5, #7, #8, #10 and #12) were found to produce clearance zone ratios that were larger than or similar to those observed with the V212T YebF-LCC control (Fig. 4A). Following triplicate measurements to assess variability in clearance-zone ratios, colony #10 produced the largest clearance zone, and colony #1 produced the second-largest (Fig. 4B and Fig. S7). Sequencing of plasmids isolated from colonies #10 and #1 revealed that they encoded V212T-L102F and V212T-L102A, respectively.

As a final comparison, we examined the effect of YebF on the sensitivity of the plate assay. As observed for wild type LCC and the corresponding YebF fusion (Fig. 1D), *E. coli* colonies expressing the selected LCC variants form larger zones of clearances relative to YebF-fused variants (Fig. S8). However, there is no significant difference in the size of the zone of clearance, and the colony morphology is highly variable, suggesting cell lysis. In contrast, YebF-LCC variants produce consistent colony size and zones of clearances although their protein expression levels were very low as shown by SDS-PAGE (Fig. S9). Therefore, secreted enzymes linked to YebF result in zones of clearances that are more sensitive to relative enzyme activity. While some esterases, including LCC, have promiscuous cell-lysing activities that could be exploited for on-plate activity screening without the need for a secretion signal,[47] the YebF-based assay described here enables zone-clearance activity screens to be extended to other plastic-degrading hydrolases that lack this activity (*e.g.*: nylonases, polyurethanases).[48,49]

The stability of a biocatalyst is an important feature for industrial applications. This is also the case for enzymatic PET hydrolysis, where the enzyme must be sufficiently thermostable to work at reaction temperatures near the glass transition temperature (T_g) of PET ($T_g \sim 70$ °C),[50] where the polymer chains become more mobile and accessible to the enzyme. Recrystallization of PET also occurs rapidly at the T_g and competes with enzymatic depolymerization. For this reason,

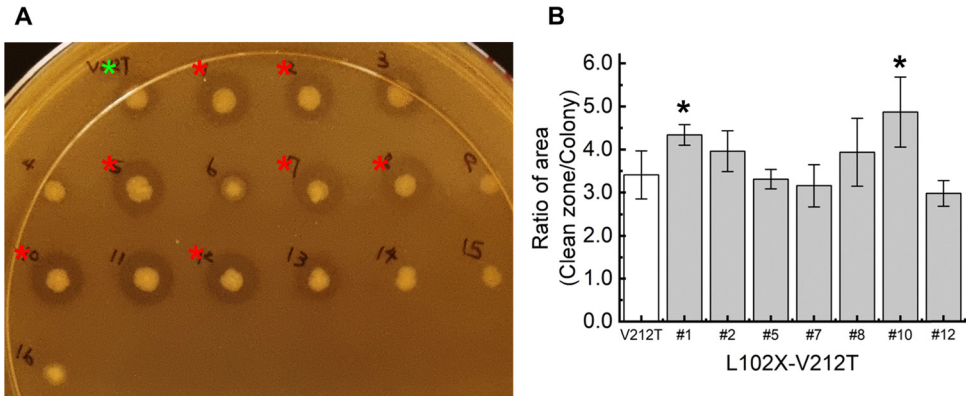

Fig. 4 Screening YebF-LCC V212T-L102X variants using a BHET zone clearing assay. (A) *E. coli* colonies expressing YebF-LCC-V212T variants derived from site-saturating mutagenesis at position L102 were incubated on LB auto-induction agar plates supplemented with 0.025% glycine and 5 mM BHET. The plates were incubated at 30 °C for one day, followed by 42 °C for one day. The areas of the clearance zones and the corresponding colonies were measured with ImageJ and expressed as ratios (Fig. S7A). A variant with a zone of clearance/colony size ratio that is greater than that of the YebF-LCC V212T control (green asterisk) is marked with a red asterisk. (B) Selected *E. coli* colonies expressing more active V212T-L102X variants were used to inoculate LB-agar-BHET plates. The mutants with the highest and second-highest ratios were marked. Zone clearance ratios were measured in triplicate (Fig. S7B).

PETase reactions are typically run at a slightly lower temperature of 68 °C, which minimizes recrystallization and maintains the amorphous form of the polymer that is more accessible to the enzyme.[51] To evaluate the impact of the substitutions identified in this work on the thermostability of the LCC variants, T_m values of purified LCC variants were measured using the differential absorbance of Trp residues in the folded and unfolded states. The L102F and L102F–V212T variants of LCC exhibit progressively lower T_m values relative to the WT enzyme (Fig. S10). The observed decreases in T_m likely reflect subtle structural rearrangements near the substrate-binding pocket that enhance enzymatic activity while compromising global stability, a phenomenon commonly observed in directed evolution.[52,53] However, the decreases in T_m are modest (from 93 °C to 81 °C) and the T_m of each enzyme remained well above the optimal reaction temperature with PET (68 °C). Additional experiments will be required to conclusively demonstrate that gains in activity observed at 45 °C with the LCC variants found here will show corresponding enhancements at temperatures nearer to the T_g of PET.

To confirm the results of the YebF-mediated secretion screen, LCC and the V212T and L102F–V212T variants lacking the YebF tag were expressed, purified, and subjected to *in vitro* assays. First, kinetic parameters were determined for the enzyme-catalyzed hydrolysis of *p*NPB. With this substrate, all enzymes exhibited similar k_{cat} values, whereas the K_M value for LCC L102F–V212T (148 μM) increased slightly relative to WT (114 μM) and the V212T variant (127 μM). Consequentially, the k_{cat}/K_M for the L102F–V212T variant is 60% that of V212T and 67% that of the WT enzyme (Table 1 and Fig. S11). Although the relative activities towards *p*NPB do not align with the increased activities observed with the zone clearance screen against BHET, the major structural differences between these two substrates likely lead to differences in active-site binding interactions.[4,54] Consequently, mutations that enhance PET hydrolysis may have little effect on, or even impair, activity towards small ester substrates. This observation underscores the necessity of substrate-relevant screening systems in enzyme engineering, particularly for polymer-degrading enzymes where catalytic efficiency is likely governed more by surface adsorption and hydrophobic interactions rather than classical Michaelis–Menten kinetics.[4,55]

Table 1 Kinetic parameters for the hydrolysis of *p*NPB by wild-type (WT) LCC and its variants in 50 mM citrate, 100 mM phosphate (pH 8.0) at 45 °C. The k_{cat} and K_M values were determined with the Michaelis–Menten equation (Fig. S11)

Enzyme	k_{cat} (s^{-1})	K_M (μM)	k_{cat}/K_M (s^{-1} mM^{-1})
WT	45.8 ± 1.7	48.8 ± 2.3	(9.39 ± 0.19) × 10^2
V212T	51.9 ± 4.3	49.7 ± 8.0	(10.5 ± 0.85) × 10^2
L102F–V212T	42.4 ± 0.4	67.7 ± 1.5	(6.27 ± 0.19) × 10^2

While BHET is not a perfect mimic of PET, as an intermediate of PET depolymerization it has the potential to select for enzymes that are efficient in either BHET or PET hydrolysis. Therefore, LCC variants selected against BHET must be assayed against PET to evaluate whether enhanced activities against the proxy substrate truly translated into enhanced activity on the authentic polymer substrate. Accordingly, we next compared the activities of the LCC variants towards BHET and bis(benzoyloxyethyl) terephthalate (3PET) *in vitro*. Both BHET and 3PET are poorly soluble in buffered solution, whereas the products released upon ester hydrolysis are water soluble. This property permits rates of BHET and 3PET hydrolysis to be monitored by following decreases in turbidity over time. When LCC L102F–V212T was assayed with a suspension of BHET, rates of clearance were found to be 2.0 and 1.1-fold faster than with WT and the V212T variant (Fig. 5), respectively, in good agreement with the results of the on-plate screen (Fig. 2B and Fig. 4B). Taken together with the results obtained with *p*NPB

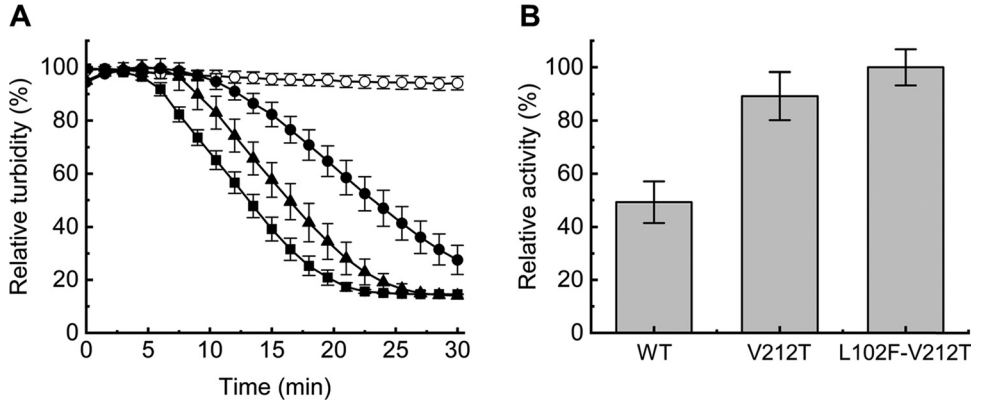

Fig. 5 Turbidity-based assay for hydrolytic activity of LCC variants toward BHET. (A) Time-dependent changes in turbidity were monitored for blank controls (open circles), wild-type LCC (WT, circles) and its variants V212T (triangles) and L102F–V212T (squares). (B) Initial reaction rates derived from turbidity measurements are shown for WT, as well as the V212T, and L102F-V212T variants. Reactions were conducted in 50 mM citrate, 100 mM phosphate buffer (pH 8.0) containing 5 mM BHET and 800 nM enzyme, incubated at 45 °C for 30 minutes. Turbidity was measured at 600 nm. Blank contained bovine serum albumin (BSA) with the same enzyme concentration. All experiments were performed in triplicate.

(Fig. S11), this demonstrates the importance of screening against substrates that mimic the true target molecule. The selected variants were next assayed with 3PET, a mimic of a PET trimer.[56] The rate of clearance corresponding to 3PET hydrolysis was 1.5- and 1.3-fold faster with L102F–V212T compared to V212T and the WT enzyme, respectively (Fig. 6A and B). Initial rates measured by this assay were also collected at various concentrations of 3PET and the apparent sigmoidal dependence of rate *versus* substrate concentration necessitated analysis of these data using the Hill equation (Fig. S12). Fitting initial rates of 3PET hydrolysis collected for each enzyme to this equation permitted derivation of the kinetic parameters shown in Table 2. These results reveal that both k_{cat} and k_{cat}/K_M for 3PET hydrolysis are higher with L102F–V212T than with the WT or V212T variant. The observed increases in these parameters are modest, and the increased value of K_M for the L102F–V212T mutant suggests that substrate binding is perturbed relative to the WT enzyme. As such, the improved k_{cat}/K_M observed with the L102F–V212T is the result of the enhanced k_{cat} offsetting the increased K_M value, potentially reflecting that the mutations primarily improve turnover and not affinity for the substrate. In contrast, the differences *n*-values are not statistically significant, indicating that the apparent cooperative effect in 3PET hydrolysis was not perturbed by the active site substitutions.

Table 2 Kinetic parameters for the hydrolysis of 3PET by wild-type (WT) LCC and its variants in 50 mM citrate, 100 mM phosphate (pH 8.0) at 45 °C. The k_{cat}, K_M, and *n*-values were determined with the Hill equation (Fig. S12)

Enzyme	k_{cat} (s^{-1})	K_M (μM)	k_{cat}/K_M (s^{-1} mM^{-1})	*n*-value
WT	4.04 ± 0.31	114 ± 12	35.6 ± 1.4	1.60 ± 0.09
V212T	4.77 ± 0.13	127 ± 14	36.5 ± 1.3	1.58 ± 0.12
L102F–V212T	6.73 ± 0.14	148.0 ± 2.1	45.4 ± 0.6	1.530 ± 0.066

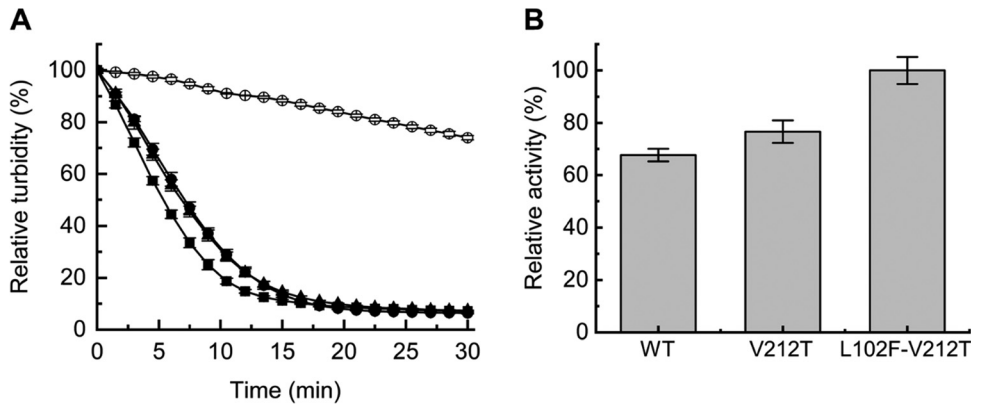

Fig. 6 Turbidity-based assay for hydrolytic activity of LCC variants toward 3PET. (A) Time-dependent turbidity changes were monitored for blank controls (open circles), wild-type LCC (WT, circles), and variants V212T (triangles) and L102F–V212T (squares). (B) Initial reaction rates derived from turbidity measurements are shown for WT, as well as the V212T and L102F-V212T variants. Reactions were carried out in 50 mM citrate, 100 mM phosphate buffer (pH 8.0) containing 350 μM 3PET, incubated at 45 °C for 30 minutes. Blank contained bovine serum albumin (BSA) with the same enzyme concentration. All experiments were performed in triplicate.

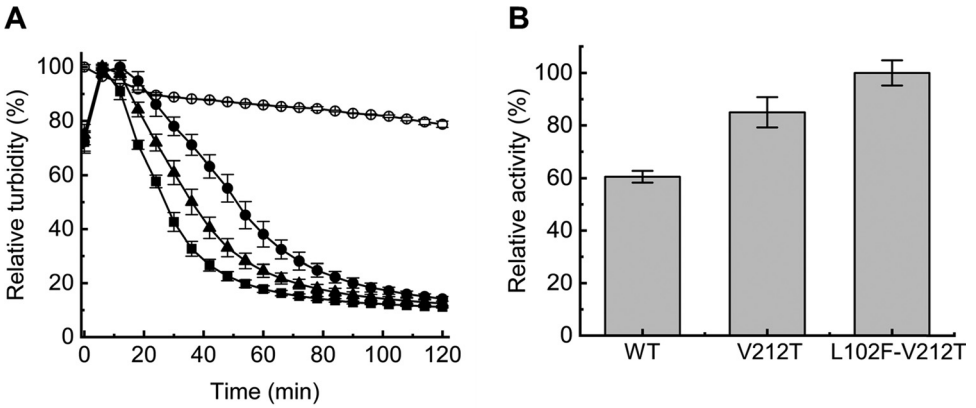

Fig. 7 Turbidity-based assay for hydrolytic activity of LCC variants toward PET nanoparticles. (A) Time-dependent changes in turbidity were monitored for Blank controls (open circles), wild-type LCC (WT, circles) and its variants V212T (triangles) and L102F–V212T (squares). (B) Initial reaction rates derived from turbidity measurements are shown for WT, V212T, and L102F-V212T variants. Reactions were conducted in 10 mM citrate, 20 mM phosphate buffer (pH 8.0) containing 0.50 mg mL^{-1} PET nanoparticles and 1.73 μM enzyme, incubated at 45 °C for 2 h. Turbidity was measured at 600 nm. Blank contained bovine serum albumin (BSA) with the same enzyme concentration. All experiments were performed in triplicate.

To further validate the selection of LCC variants, PET nanoparticles (NPs) were prepared and tested as substrates using a turbidity assay. The L102F–V212T variant was observed to clarify PET NP emulsions 1.7 and 1.2-fold faster relative to WT and the V212T variant, respectively (Fig. 7). The greater activity of the L102F–V212T variant towards PET NPs mirrors the similar enhanced activity towards BHET and 3PET as substrates. This result further validates the use of the YebF-mediated secretion-based screen with BHET-amended solid media plates to effectively identify substitutions that improve activity against PET. Overall, these findings underscore the utility of secretion-based screening platforms in guiding both rational design and evolutionary optimization of polyester hydrolases.

To examine the influence of the selected substitutions on PET hydrolysis at a molecular level, LCC, V212T, and L102F–V212T variants were modelled bound to 3PET. These models suggested that the conformation of H242, a critical component of the catalytic triad (Ser165-His242-Asp210),[57,58] is influenced by the positioning of V212 (Fig. S13A and B). Two different binding modes were identified in LCC, wherein V212 adopted one of two conformations: a ''horizontal'' orientation that preserves the key H-bonding interactions between the residues that comprise the catalytic triad, and a ''vertical'' orientation, where the sidechain of V212 disrupts the interaction between H242 and D210. Glide scores for these modes were very similar (Fig. S14), suggesting that the two conformations would occur with similar propensity. Given the disrupted catalytic triad, the ''vertical'' mode was assumed to be less favourable for PET hydrolysis, as precise histidine positioning is essential for proton shuttling during catalysis.[57,59,60] With both V212T and L102F–V212T variants, the V212T residue also adopted two different conformations, but the catalytic triad was not perturbed in either conformer. This suggests that the V212T substitution improved activity by eliminating the non-productive binding mode wherein the catalytic machinery is disrupted (Fig. S13C and D).

Interestingly, the binding affinities of the V212T and L102F–V212T variants for 3PET, as approximated by the Glide score, are lower than that of the WT in both binding modes.[37,38] This is consistent with the observed increases in K_M for this substrate (Table 2). However, the vertical orientation of V212T in the variant PETases enables the carbonyl of the scissile bond of 3PET to bind nearer the catalytic S165 nucleophile, potentially reflecting a more productive orientation for catalysis (Fig. S13). This spatial proximity may facilitate nucleophilic attack and improve catalytic turnover (k_{cat}), as previously reported for other PETases that exhibit enhanced transition state alignment despite similar or weaker ground state binding.[61,62] Notably, the binding behaviour of V212T differs markedly between the V212T and L102F–V212T variants, with substantial differences in binding affinity between its vertical and horizontal conformations (Fig. S13). In the V212T variant, the Thr sidechain predominantly adopts a 'horizontal' conformation, which is predicted to enhance substrate binding, but results in suboptimal alignment with the nucleophilic S165. This variant can also form a 'vertical' conformation that improves alignment with S165, although this state is predicted to exhibit lower affinity to the substrate. Conversely, the L102F–V212T mutant preferentially stabilizes the 'vertical' conformation of T212, which not only enhances alignment with S165 but also achieves higher binding affinity than its horizontal counterpart. These conformational preferences likely contribute to the increased k_{cat} observed in both mutants, as improved transition state stabilization can compensate for modest changes in ground state binding (Table 2).

The impact of the L102F substitution appears to be more subtle. The L102F substitution alone does not appear to directly affect the active site conformations but may enhance local surface stability through increased hydrophobic interactions. A surface analysis indicates that the overall hydrophobicity (as gauged by the hydrophobic moment) of the L102F–V212T variant increased compared to WT and V212T (Fig. S15A and S16), despite the positive and negative surface areas of the L102F–V212T variant remaining nearly identical to those of WT (Fig. S15 and S16). The elevated hydrophobic moment in the

L102F–V212T variant suggests a more compact and less hydrated substrate-binding pocket, potentially improving accommodation of the hydrophobic PET structure. This aligns with previous findings that moderate increases in surface hydrophobicity can enhance PET adsorption and promote productive binding without compromising protein solubility.[63–65]

Overall, the results of these docking studies point to very subtle, cooperative effects of V212T and L102F substitutions that alter both the binding orientations and surface hydrophobicity of LCC, thereby enhancing substrate positioning for hydrolysis. Local structural tuning, particularly around residues influencing the catalytic histidine orientation and hydrophobic surface distribution, may represent a promising strategy for the rational engineering of PET hydrolases with improved catalytic efficiency.

Conclusions

In this study, we developed a YebF-mediated secretion-based assay in *E. coli* for rapid, on-plate screening of PETase variants. Optimization of secretion conditions demonstrated that YebF enables efficient extracellular release of active LCC in LB media, particularly when supplemented with low concentrations of glycine. The resulting plate-based assay allowed direct visualization of PETase activity *via* zone clearance without requiring cell lysis or protein purification. This work establishes a simple and effective secretion-based on-plate screening platform for directed evolution of polyester hydrolases. Using this platform, site-saturation mutagenesis and iterative screening identified two key substitutions, L102F and V212T, that synergistically enhanced PET-degrading activity. Relative to the WT LCC, the L102F–V212T double mutant exhibited accelerated hydrolysis of BHET, 3PET, and PET nanoparticles, confirming the reliability of this assay to identify variants with enhanced kinetic parameters. Structural modelling suggests that V212T stabilizes an active conformation of residues comprising the catalytic triad, while L102F may increase local hydrophobicity, collectively enhancing substrate positioning and turnover. Although the double mutant identified in this work exhibits modest improvements over the parent enzyme, the YebF-mediated approach provides a time- and resource-efficient route that could easily be used to evaluate PETase mutants more broadly to identify variants with enhanced activity. Finally, the YebF on-plate screening approach can in principle be extended to discovering or engineering enzymes that target a variety of polyesters,[66] nylon,[67] certain polyurethanes (e.g.: Impranil),[68] and other plastic polymers or oligomers of interest that can form dispersions in agar media. Work to this effect is ongoing in our labs.

Materials and methods

General

The plasmid pD421-yebF-LCC was synthesized by ATUM Biosciences and encodes LCC with an *N*-terminal YebF sequence and a *C*-terminal His_6 tag (Fig. S17 and S18). Protein expression was performed in *Escherichia coli* BL21 (DE3) in the following media, each containing 50 μg mL^{-1} kanamycin: Luria-Bertani broth (LB; 10 g L^{-1} tryptone, 5.0 g L^{-1} yeast extract, 10 g L^{-1} NaCl); terrific broth (TB; 12 g L^{-1} tryptone, 24 g L^{-1} yeast extract); and super broth (SB; 35 g L^{-1} tryptone, 20 g L^{-1} yeast extract). For autoinduction, each of these media additionally contained 0.3 g L^{-1} $MgSO_4 \cdot 6H_2O$, 3.3 g L^{-1} $(NH_4)_2SO_4$, 6.8 g L^{-1} KH_2PO_4, 7.1 g L^{-1} Na_2HPO_4, 0.5 g L^{-1} D-glucose, and 2.0 g L^{-1} lactose. Solid media plates were prepared with 15 g L^{-1} agar. The pH of the media was adjusted to pH 7.0 or 7.5 prior to autoclaving. For optimization of glycine concentration for the secretion-based zone-clearing assay, autoinduction LB agar plates contained 0.025% to 0.4% (m/v) glycine and 5 mM bis(2-hydroxyethyl) terephthalate (BHET) (Sigma-Adrich, ON, Canada).

YebF-mediated secretion of LCC in autoinduction media

Chemically competent *E. coli* BL21 (DE3) cells were transformed with pD421-yebF-LCC. Transformants were plated on LB agar plates and grown overnight at 37 °C. A single colony was then used to inoculate 10 mL of sterile LB that was grown overnight at 37 °C and 180 rpm. A 200 μL aliquot of the overnight culture was then used to inoculate 20 mL of LB, TB, or SB auto-induction media. Each culture was incubated at 30 °C for 24 h at 180 rpm. The supernatant and the cells were collected by centrifugation (5000 × *g*, 10 min, 4 °C). After resuspending the collected cells in 20 mM sodium phosphate (pH 7.5), lysis was performed using a Qsonica Q500 set to 30% amplitude, with cycles of 3 s on, 2 s off for 10 minutes. The insoluble material was removed by centrifugation at 17 000 × *g* for 30 min at 4 °C. The protein concentration was determined using the Quick Start™ Bradford Protein Assay (Bio-Rad, CA, USA). The esterase activities of the supernatant and the soluble protein were measured by monitoring the hydrolysis of *p*-nitrophenyl butyrate (*p*NPB) (Sigma-Aldrich, ON, Canada), as described below.

Site saturation mutagenesis of YebF-LCC

HotSpot Wizard was used to select the active site residues Y95, L102, and V212 of LCC for site saturation mutagenesis using the degenerate primers listed in Table S1.[69] The mutagenic PCR reactions contained 7 ng template DNA (pD421-yebF-LCC for single mutants or pD421-yebF-LCC-V212T for double mutants), 0.2 mM dNTPs, 0.5 μM forward and reverse primers, and 0.02 U μL^{-1} Phusion™ DNA polymerase in Phusion™ HF buffer. The PCR mixture was heated for 3 min at 98 °C, followed by 18 cycles of 30 s at 98 °C, 30 s at 68 °C, and 6 min at 72 °C. Finally, the PCR mixtures were treated with DpnI (20 U) for 2 h at 37 °C before being transformed into chemically competent *E. coli* DH10β cells. The transformed cells were grown overnight on LB agar plates, and the resulting colonies were pooled and cultured overnight in LB media. Pooled plasmid DNA was then isolated using the Monarch Plasmid Miniprep Kit (New England Biolabs, ME, USA) according to the manufacturer's instructions.

Zone clearing assay to screen for YebF-LCC variants

Pooled plasmid mixtures were transformed into chemically competent *E. coli* BL21 (DE3), and the transformants were grown overnight on LB agar plates. Single colonies were then picked and transferred to LB autoinduction agar plates doped with 5 mM BHET and 0.025% glycine showing large zone of clearance in the glycine optimization (Fig. 1B). The plates were then incubated at 30 °C for 24 h before further incubation at 42 °C for 24 h. To precisely confirm the enhanced hydrolytic activity of YebF-LCC variants, colonies producing larger zones of clearance than WT or V212T were selected to inoculate LB and incubated at 37 °C at 180 rpm for 6 h under identical growth conditions, standardized by OD_{600} measurements.[3] Aliquots of the cultures (1.5 μL) were then spotted onto LB autoinduction agar plates containing 5 mM BHET and 0.025% glycine and incubated again at 30 °C for 24 h, then 42 °C for 24 h. For each colony, the area of the clearance zone and colony were measured using ImageJ, and the ratio of the clearance zone area to that of the overexpressing colony was taken as a normalized measure of clearance.

Deletion of the YebF sequence from YebF-LCC and variants

YebF secretion tags were removed from LCC variants by amplifying the DNA sequence encoding the PETase from the corresponding plasmid using the primers given in Table S2. Briefly, PCR reactions contained 50 ng of template DNA, 0.2 mM dNTP, 0.5 μM of each primer, and 0.02 U μL^{-1} Phusion™ DNA polymerase in Phusion™ HF buffer. After initial denaturation at 98 °C for 3 min, 34 cycles of 98 °C for 30 s, 65 °C for 30 s, and 72 °C for 6 min were followed by a final extension period of 10 min at 72 °C. Amplicons were digested with *Nco*I and *Xho*I before being ligated into a pET-28a(+) vector that had been digested by the same restriction enzymes, yielding pET28-LCC, pET28-LCC-V212T, and pET28-LCC-L102F–V212T.

Overexpression and purification of LCC variants

A single colony of *E. coli* BL21 (DE3) transformed with pET28-LCC, pET28-LCC-V212T, or pET28-LCC-L102F–V212T was used to inoculate a 5 mL overnight culture in LB that was then grown at 37 °C and 180 rpm. These cultures were used to inoculate 100 mL of LB, followed by growth at 37 °C and 180 rpm until the OD_{600} reached 0.6–0.8. Expression was then induced by the addition of isopropyl β-D-1-thiogalactopyranoside (IPTG) to a final concentration of 0.1 mM. The cultures were then incubated at 25 °C and 180 rpm for a further 24 h. The cells were collected by centrifugation at 5000 × *g* for 10 min at 4 °C before being resuspended in 10 mL of Buffer A (10 mM imidazole, 300 mM NaCl, 50 mM Tris-HCl, pH 7.5). Cells were lysed on ice with a Qsonica Q500 Sonicator set to 30% amplitude using cycles of 3 s on and 2 s off over 10 min before the insoluble material was removed by centrifugation at 17 000 × *g* for 30 min at 4 °C. The supernatant was loaded onto a HisTrap HP Ni-NTA column (Cytiva, BC, Canada) that was pre-equilibrated with Buffer A. After washing the column with 10 column volumes of Buffer A, the LCC variants were eluted with a step gradient from 20 mM to 500 mM imidazole in 50 mM Tris-HCl, 500 mM NaCl, pH 7.5. All elution fractions were analysed by SDS-PAGE. Fractions containing the LCC were combined and buffer exchanged into 20 mM sodium phosphate, pH 7.5 using a HiTrap SP HP cation exchange column (Cytiva, BC, Canada) and a linear gradient of 50 mM to 1000 mM NaCl in 20 mM sodium phosphate, pH 7.5.

Melting temperature analysis

The melting temperature (T_m) of each LCC variant was measured by monitoring the change in absorbance at 280 nm (A_{280}) as a function of temperature. LCC variants (0.2 mg mL^{-1}) in 100 μL 20 mM sodium phosphate (pH 7.5) were placed in a quartz cuvette. Samples were heated from 25 °C to 105 °C at a rate of 5 °C min^{-1} while monitoring the absorbance at 280 nm with 2 nm spectral bandwidth every 0.1 s using the Multicell Peltier heating block of a Cary 3500 UV-vis system (Agilent, CA, USA). Plots of the first derivative of A_{280} as a function of temperature were used to determine T_m values, with the maximal value corresponding to the melting temperature.[70]

Esterase activity assays using *p*NPB

The esterase activities of purified LCC and variants thereof were measured by reacting 1 mM *p*NPB with 0.5 nM enzyme in buffer comprised of 50 mM citrate and 100 mM phosphate buffer (pH 8.0) at 45 °C. Reactions were conducted in 96-well plates, and the absorbance at 405 nm was recorded as a function of time with a Spectramax® M2 microplate reader (Molecular Devices, CA, USA). Specific activity was defined as the amount of *p*-nitrophenolate released (nmol) per minute per milligram of protein. Initial rates at each *p*NPB concentration were measured and fit to the Michaelis–Menten equation using OriginPro 2024 (OriginLab Corporation, MA, USA):

$$v = \frac{k_{cat}[E]_0 \times [S]}{K_M + [S]}$$

where v is the initial reaction velocity, [S] is the substrate concentration, k_{cat} is the turnover number, $[E]_0$ is the total enzyme concentration, and K_M is the Michaelis constant. Non-linear curve fitting was performed using Origin's built-in fitting module, and kinetic parameters were extracted accordingly.

Turbidity assays with BHET, 3PET, and PET nanoparticles

Bis(benzoyloxyethyl) terephthalate (3PET) was synthesized and purified as described previously.[56] Solutions of 1 M BHET and 90 mM 3PET were prepared in DMSO and diluted into 50 mM citrate, 100 mM phosphate (pH 8.0). Enzyme activity against BHET (5 mM) and 3PET (350 μM) was monitored at 45 °C by measuring the change of turbidity at 600 nm (A_{600}) in a 96-well plate. Reactions were monitored by following A_{600} for 30 min after the addition of 0.8 μM and 0.1 μM LCC variant for BHET and 3PET, respectively.

To prepare PET nanoparticles, 0.2 g of granulated PET (Sigma-Adrich, ON, Canada) was dissolved in 10 mL 1,1,1,3,3,3-hexafluoro-2-propanol (HFIP). The solution was slowly added to a glass beaker containing 100 mL of ice-cold

H_2O with vigorous stirring.[71] The HFIP was removed by heating the suspension at 65 °C with stirring overnight. The concentration of PET nanoparticles was determined by weight after drying a fixed volume of the PET nanoparticle suspension at 40 °C overnight. Each LCC variant (2 μM) was incubated with 0.5 mg mL^{-1} PET nanoparticles in 20 mM citrate/phosphate buffer (pH 8.0) at 45 °C for 2 h. The change of turbidity was measured over time at 600 nm in a 96-well plate.

Kinetic analysis for 3PET

A 90 mM stock solution of 3PET in DMSO was diluted to final concentrations ranging from 25 to 350 μM in 50 mM citrate, 100 mM phosphate buffer (pH 8.0). Enzymatic hydrolysis of 3PET was initiated by adding 0.1 μM LCC variants, and activity was monitored by measuring at A_{600} for 2 h at 45 °C in a 96-well plate. Initial rates at each 3PET concentration were fit to the Hill equation using OriginPro 2024:

$$v = \frac{k_{cat}[E]_0 \times [S]^n}{K_d{}^n + [S]^n}$$

where v is the initial reaction velocity, [S] is the substrate concentration, k_{cat} is the turnover number, $[E]_0$ is the enzyme concentration, K_d is the apparent dissociation constant, and n is the Hill coefficient that reflects the degree of cooperativity exhibited by the enzyme being analyzed. Non-linear curve fitting was performed using Origin's built-in fitting module, and kinetic parameters were extracted accordingly.

Docking models of LCC mutants for 3PET

The structure of LCC and its variants were predicted using the AlphaFold server powered by AlphaFold3.[72] Structural alignment and root mean square deviation (RMSD) calculations relative to the LCC crystal structure (PDB: 4EB0) were performed using Wincoot (Fig. S19).[73] Complexes of 3PET with each protein were assembled and prepared in Schrödinger Suite.[74–76] Both protein and ligand structures were optimized at pH 8.0 ± 2.0 using the OPLS4 force field. Docking was performed *via* induced fit docking (IFD) in Maestro, targeting the centroid residue Ser165. A docking box of 25 × 25 × 25 $Å^3$ was defined, and residues within 5 Å of the ligand were refined during the docking process.

Author contributions

Jaeick Lee: conceptualization, formal analysis, investigation, methodology, visualization, writing – original draft, editing. Maame Yaa Yamoa: investigation, methodology. Celina L. Bradley: investigation, methodology. Graeme Howe: supervision, validation, funding acquisition, writing – original draft, writing – review, editing. David L. Zechel: conceptualization, project administration, supervision, validation, funding acquisition, writing – original draft, writing – review & editing.

Conflicts of interest

The authors declare no competing interests.

Data availability

All relevant data are contained within the manuscript and its supplementary information (SI). Supplementary information (SI) is available. See DOI: https://doi.org/10.1039/d6cb00090h.

Acknowledgements

We are grateful to Zhenyu Hu for providing the 3PET substrate. GWH and DLZ are grateful for support from the Natural Sciences and Engineering Council of Canada (GWH: RGPIN-2020-0445, DLZ: RGPIN-2025-04520), Ontario Genomics (OGI-207), and the Genome Canada Large Scale Applied Research Program.

References

1 H. S. Zurier and J. M. Goddard, *Biotechnol. Bioeng.*, 2023, **120**, 1000–1014.
2 T. R. Walker and L. Fequet, *TrAC, Trends Anal. Chem.*, 2023, **160**, 116984.
3 X. Wang, C. Song, Q. Qi, Y. Zhang, R. Li and L. Huo, *Eng. Microbiol.*, 2022, **2**, 100020.
4 V. Pirillo, L. Pollegioni and G. Molla, *FEBS J.*, 2021, **288**, 4730–4745.
5 V. Tournier, C. M. Topham, A. Gilles, B. David, C. Folgoas, E. Moya-Leclair, E. Kamionka, M.-L. Desrousseaux, H. Texier, S. Gavalda, M. Cot, E. Guémard, M. Dalibey, J. Nomme, G. Cioci, S. Barbe, M. Chateau, I. André, S. Duquesne and A. Marty, *Nature*, 2020, **580**, 216–219.
6 C. Sonnendecker, J. Oeser, P. K. Richter, P. Hille, Z. Zhao, C. Fischer, H. Lippold, P. Blázquez-Sánchez, F. Engelberger, C. A. Ramírez-Sarmiento, T. Oeser, Y. Lihanova, R. Frank, H.-G. Jahnke, S. Billig, B. Abel, N. Sträter, J. Matysik and W. Zimmermann, *ChemSusChem*, 2022, **15**, e202101062.
7 P. C. F. Buchholz, G. Feuerriegel, H. Zhang, P. Perez-Garcia, L.-L. Nover, J. Chow, W. R. Streit and J. Pleiss, *Proteins: Struct., Funct., Bioinf.*, 2022, **90**, 1443–1456.
8 R. Wei, G. von Haugwitz, L. Pfaff, J. Mican, C. P. S. Badenhorst, W. Liu, G. Weber, H. P. Austin, D. Bednar, J. Damborsky and U. T. Bornscheuer, *ACS Catal.*, 2022, **12**, 3382–3396.
9 E. L. Bell, R. Smithson, S. Kilbride, J. Foster, F. J. Hardy, S. Ramachandran, A. A. Tedstone, S. J. Haigh, A. A. Garforth, P. J. R. Day, C. Levy, M. P. Shaver and A. P. Green, *Nat. Catal.*, 2022, **5**, 673–681.
10 T. M. Groseclose, E. A. Kober, M. Clark, B. Moore, S. Banerjee, V. Bemmer, G. T. Beckham, A. R. Pickford, T. T. Dale and H. B. Nguyen, *ACS Catal.*, 2024, **14**, 14622–14638.
11 S. Sulaiman, S. Yamato, E. Kanaya, J.-J. Kim, Y. Koga, K. Takano and S. Kanaya, *Appl. Environ. Microbiol.*, 2012, **78**, 1556–1562.
12 S. Brott, L. Pfaff, J. Schuricht, J.-N. Schwarz, D. Böttcher, C. P. S. Badenhorst, R. Wei and U. T. Bornscheuer, *Eng. Life Sci.*, 2022, **22**, 192–203.

13 T. M. Groseclose, E. Kober, M. Clark, B. Moore, R. K. Jha, Z. K. Taylor, L. A. Lujan, G. T. Beckham, A. R. Pickford, T. Dale and H. B. Nguyen, *Chem. Catal.*, 2025, 101399.
14 G. Taxeidis, M. Djapovic, E. Nikolaivits, V. Maslak, J. Nikodinovic-Runic and E. Topakas, *ACS Sustainable Chem. Eng.*, 2024, **12**, 5943–5952.
15 M. A. Cribari, M. J. Unger, I. C. Unarta, A. N. Ogorek, X. Huang and J. D. Martell, *J. Am. Chem. Soc.*, 2023, **145**, 27380–27389.
16 M. Hajighasemi, A. Tchigvintsev, B. Nocek, R. Flick, A. Popovic, T. Hai, A. N. Khusnutdinova, G. Brown, X. Xu, H. Cui, J. Anstett, T. N. Chernikova, T. Brüls, D. Le Paslier, M. M. Yakimov, A. Joachimiak, O. V. Golyshina, A. Savchenko, P. N. Golyshin, E. A. Edwards and A. F. Yakunin, *Environ. Sci. Technol.*, 2018, **52**, 12388–12401.
17 R. Molitor, A. Bollinger, S. Kubicki, A. Loeschcke, K.-E. Jaeger and S. Thies, *Microbial. Biotechnol.*, 2020, **13**, 274–284.
18 H. Seo, S. Kim, H. F. Son, H.-Y. Sagong, S. Joo and K.-J. Kim, *Biochem. Biophys. Res. Commun.*, 2019, **508**, 250–255.
19 L. Shi, H. Liu, S. Gao, Y. Weng and L. Zhu, *J. Agric. Food Chem.*, 2021, **69**, 2245–2252.
20 X. Li, B. Shi, J.-W. Huang, Z. Zeng, Y. Yang, L. Zhang, J. Min, C.-C. Chen and R.-T. Guo, *Bioresour. Bioprocess.*, 2023, **10**, 26.
21 Y. Branson, C. P. S. Badenhorst, L. Pfaff, C. Buchmann, R. Wei and U. T. Bornscheuer, in *Metagenomics: Methods and Protocols*, ed W. R. Streit and R. Daniel, Springer US, New York, NY, 2023, pp. 153–165.
22 L. Aer, H. Qin, P. Wo, J. Feng and L. Tang, *Bioresour. Technol.*, 2024, **391**, 129884.
23 R. Wei, T. Oeser, S. Billig and W. Zimmermann, *Biotechnol. J.*, 2012, **7**, 1517–1521.
24 G. R. M. Kleiner-Grote, J. M. Risse and K. Friehs, *Eng. Life Sci.*, 2018, **18**, 532–550.
25 S. R. Lokireddy, S. R. Kunchala and R. Vadde, *World J. Microbiol. Biotechnol.*, 2025, **41**, 90.
26 F. Baneyx and M. Mujacic, *Nat. Biotechnol.*, 2004, **22**, 1399–1408.
27 G. Zhang, S. Brokx and J. H. Weiner, *Nat. Biotechnol.*, 2006, **24**, 100–104.
28 A. Tsirigotaki, J. De Geyter, N. Šoštaric, A. Economou and S. Karamanou, *Nat. Rev. Microbiol.*, 2017, **15**, 21–36.
29 G. Koteswara Reddy, T. Manas and B. Devi Sri Siddhartha, in *Impact of Petroleum Waste on Environmental Pollution and its Sustainable Management Through Circular Economy*, ed I. D. Behera and A. P. Das, Springer Nature Switzerland, Cham, 2023, pp. 235–251.
30 L. Brivio, S. Meini, M. Sponchioni and D. Moscatelli, *Chem. Eng. Sci.*, 2024, **284**, 119466.
31 T. M. Groseclose and H. B. Nguyen, *Commun. Mater.*, 2025, **6**, 190.
32 J. G. Owen, J. N. Copp and D. F. Ackerley, *Biochem. J.*, 2011, **436**, 709–717.
33 J. Yang, T. Moyana, S. MacKenzie, Q. Xia and J. Xiang, *Appl. Environ. Microbiol.*, 1998, **64**, 2869–2874.
34 B. Li, L. Wang, L. Su, S. Chen, Z. Li, J. Chen and J. Wu, *Biotechnol. Bioprocess Eng.*, 2012, **17**, 1128–1134.
35 C. Zou, X. Duan and J. Wu, *Bioresour. Technol.*, 2014, **172**, 174–179.
36 Z. Li, Z. Gu, M. Wang, G. Du, J. Wu and J. Chen, *Appl. Microbiol. Biotechnol.*, 2010, **85**, 553–561.
37 R. A. Friesner, J. L. Banks, R. B. Murphy, T. A. Halgren, J. J. Klicic, D. T. Mainz, M. P. Repasky, E. H. Knoll, M. Shelley, J. K. Perry, D. E. Shaw, P. Francis and P. S. Shenkin, *J. Med. Chem.*, 2004, **47**, 1739–1749.
38 R. Meli, G. M. Morris and P. C. Biggin, *Front. Bioinform.*, 2022, **2**, 885983.
39 S. Yoshida, K. Hiraga, T. Takehana, I. Taniguchi, H. Yamaji, Y. Maeda, K. Toyohara, K. Miyamoto, Y. Kimura and K. Oda, *Science*, 2016, **351**, 1196–1199.
40 C. Li, Q. Zheng, W. Liu, Q. Zhao and L. Jiang, *3 Biotech*, 2024, **14**, 195.
41 V. Pirillo, M. Orlando, C. Battaglia, L. Pollegioni and G. Molla, *FEBS J.*, 2023, **290**, 3185–3202.
42 C. Charlier, S. Gavalda, V. Borsenberger, S. Duquesne, A. Marty, V. Tournier and G. Lippens, *Biophys. J.*, 2022, **121**, 2882–2894.
43 G. Zhang, X. Li, W. Xia, C. Zhang, S. Zheng, J. Du, N. Wang, X. Chen, G. Lv, Y. Zhao, T. Wang, Y. Pan, M. Zhang, J.-W. Huang, C.-C. Chen, S. Huang, C. Zeng, Z. Gao, J. Chen, G. Fan, X. Zhang, H. Wang, Y. Sun, J. Wu, K. Liu, R.-T. Guo and S. Li, *bioRxiv*, 2025, preprint, DOI: 10.1101/2025.08.30.673199.
44 T. Kawabata, M. Oda and F. Kawai, *J. Biosci. Bioeng.*, 2017, **124**, 28–35.
45 H. Zhang, P. Perez-Garcia, R. F. Dierkes, V. Applegate, J. Schumacher, C. M. Chibani, S. Sternagel, L. Preuss, S. Weigert, C. Schmeisser, D. Danso, J. Pleiss, A. Almeida, B. Höcker, S. J. Hallam, R. A. Schmitz, S. H. J. Smits, J. Chow and W. R. Streit, *Front. Microbiol.*, 2022, **12**, 803896.
46 H. Zhang, R. F. Dierkes, P. Perez-Garcia, E. Costanzi, J. Dittrich, P. A. Cea, M. Gurschke, V. Applegate, K. Partus, C. Schmeisser, C. Pfleger, H. Gohlke, S. H. J. Smits, J. Chow and W. R. Streit, *FEBS J.*, 2024, **291**, 70–91.
47 G. Orr, Y. Niv, M. Barakat, A. Boginya, M. Dessau and L. Afriat-Jurnou, *Biotechnol. J.*, 2024, **19**, 2400021.
48 E. L. Bell, G. Rosetto, M. A. Ingraham, K. J. Ramirez, C. Lincoln, R. W. Clarke, J. E. Gado, J. L. Lilly, K. H. Kucharzyk, E. Erickson and G. T. Beckham, *Nat. Commun.*, 2024, **15**, 1217.
49 E. E. Drufva, J. F. Cahill, P. M. B. Saint-Vincent, A. N. Williams, V. Bocharova, N. Capra, F. Meilleur, D. L. Carper, C. Bourgery, K. Miyazaki, M. Yonemura, Y. Shiraishi, J. M. Parks, M. Zhou, I. T. Dishner, J. C. Foster, S. J. Koehler, H. R. Valentino, A. Sedova, V. Kertesz, D. P. Vasileva, L. H. Hochanadel, C. A. Figg, S. Negoro, D. Kato, S. H. Chen and J. K. Michener, *Chem. Catal.*, 2025, **5**, 101418.
50 R. Wei and W. Zimmermann, *Microbial. Biotechnol.*, 2017, **10**, 1302–1307.
51 A. Karaoli, H. Tzoupis, K. D. Papavasileiou, A. G. Papadiamantis, D. G. Mintis, C. T. Kiranoudis, I. Lynch, G. Melagraki and A. Afantitis, *Int. J. Mol. Sci.*, 2025, **26**, 7682.

52 S. R. Miller, *Evol*, 2017, **71**, 1876–1887.
53 S. D. Stimple, M. D. Smith and P. M. Tessier, *AIChE J.*, 2020, **66**, e16814.
54 R. Xue, Y. Chen, H. Rong, R. Wei, Z. Cui, J. Zhou, W. Dong and M. Jiang, *Front. Bioeng. Biotechnol.*, 2021, **9**, 762854.
55 M. Furukawa, N. Kawakami, A. Tomizawa and K. Miyamoto, *Sci. Rep.*, 2019, **9**, 16038.
56 Z. Hu, K. Klupt, D. L. Zechel, Z. Jia and G. Howe, *ChemBioChem*, 2025, **26**, e202500065.
57 C.-C. Chen, X. Han, T.-P. Ko, W. Liu and R.-T. Guo, *FEBS J.*, 2018, **285**, 3717–3723.
58 C. Charlier, S. Gavalda, J. Grga, L. Perrot, V. Gabrielli, F. Löhr, J. Schörghuber, R. Lichtenecker, G. Arnal, A. Marty, V. Tournier and G. Lippens, *Biophys. J.*, 2024, **123**, 1542–1552.
59 F. Liu, T. Wang, W. Yang, Y. Zhang, Y. Gong, X. Fan, G. Wang, Z. Lu and J. Wang, *Front. Bioeng. Biotechnol.*, 2023, **11**, 1263996.
60 T. Burgin, B. C. Pollard, B. C. Knott, H. B. Mayes, M. F. Crowley, J. E. McGeehan, G. T. Beckham and H. L. Woodcock, *Commun. Chem.*, 2024, **7**, 65.
61 A. Jäckering, F. Göttsch, M. Schäffler, M. Doerr, U. T. Bornscheuer, R. Wei and B. Strodel, *JACS Au*, 2024, **4**, 4000–4012.
62 H. Wang, Y. Cun, M. Wang, X. Du, Z. Yang, H. Wang, J. Zhang, P. Wang, Y. Feng and Y. Zhu, *Commun. Biol.*, 2025, **8**, 934.
63 N. Puspitasari, S.-L. Tsai and C.-K. Lee, *Appl. Biochem. Biotechnol.*, 2021, **193**, 1284–1295.
64 Y. Jia, N. A. Samak, X. Hao, Z. Chen, Q. Wen and J. Xing, *Front. Microbiol.*, 2022, **13**, 1005480.
65 P. Paiva, E. Ippoliti, P. Carloni, P. A. Fernandes and M. J. Ramos, *Phys. Chem. Chem. Phys.*, 2025, **27**, 2139–2150.
66 M. Hajighasemi, A. Tchigvintsev, B. Nocek, R. Flick, A. Popovic, T. Hai, A. N. Khusnutdinova, G. Brown, X. Xu, H. Cui, J. Anstett, T. N. Chernikova, T. Brüls, D. Le Paslier, M. M. Yakimov, A. Joachimiak, O. V. Golyshina, A. Savchenko, P. N. Golyshin, E. A. Edwards and A. F. Yakunin, *Environ. Sci. Technol.*, 2018, **52**, 12388–12401.
67 S. Negoro, K. D-i, T. Ohki, K. Yasuhira, Y. Kawashima, K. Nagai, M. Takeo, N. Shibata, K. Kamiya and Y. Shigeta, in *Methods in Enzymology*, ed. G. Weber, U. T. Bornscheuer and R. Wei, Academic Press, 2021, vol. 648, pp. 357–389.
68 J. de Witt, R. Molitor, J. Gätgens, C. Ortmann de Percin Northumberland, L. Kruse, T. Polen, B. Wynands, K. van Goethem, S. Thies, K.-E. Jaeger and N. Wierckx, *Microbial. Biotechnol.*, 2024, **17**, e14362.
69 L. Sumbalova, J. Stourac, T. Martinek, D. Bednar and J. Damborsky, *Nucleic Acids Res.*, 2018, **46**, W356–W362.
70 N. Poklar and G. Vesnaver, *J. Chem. Educ.*, 2000, **77**, 380.
71 P. Pérez-García, D. Danso, H. Zhang, J. Chow and W. R. Streit, in *Methods in Enzymology*, ed. G. Weber, U. T. Bornscheuer and R. Wei, Academic Press, 2021, vol. 648, pp. 137–157.
72 J. Abramson, J. Adler, J. Dunger, R. Evans, T. Green, A. Pritzel, O. Ronneberger, L. Willmore, A. J. Ballard, J. Bambrick, S. W. Bodenstein, D. A. Evans, C.-C. Hung, M. O'Neill, D. Reiman, K. Tunyasuvunakool, Z. Wu, A. Žemgulytė, E. Arvaniti, C. Beattie, O. Bertolli, A. Bridgland, A. Cherepanov, M. Congreve, A. I. Cowen-Rivers, A. Cowie, M. Figurnov, F. B. Fuchs, H. Gladman, R. Jain, Y. A. Khan, C. M. R. Low, K. Perlin, A. Potapenko, P. Savy, S. Singh, A. Stecula, A. Thillaisundaram, C. Tong, S. Yakneen, E. D. Zhong, M. Zielinski, A. Žídek, V. Bapst, P. Kohli, M. Jaderberg, D. Hassabis and J. M. Jumper, *Nature*, 2024, **630**, 493–500.
73 P. Emsley, B. Lohkamp, W. G. Scott and K. Cowtan, *Acta Crystallogr., Sect. D: Biol. Crystallogr.*, 2010, **66**, 486–501.
74 W. Sherman, T. Day, M. P. Jacobson, R. A. Friesner and R. Farid, *J. Med. Chem.*, 2006, **49**, 534–553.
75 C. Lu, C. Wu, D. Ghoreishi, W. Chen, L. Wang, W. Damm, G. A. Ross, M. K. Dahlgren, E. Russell, C. D. Von Bargen, R. Abel, R. A. Friesner and E. D. Harder, *J. Chem. Theory Comput.*, 2021, **17**, 4291–4300.
76 R. C. Johnston, K. Yao, Z. Kaplan, M. Chelliah, K. Leswing, S. Seekins, S. Watts, D. Calkins, J. Chief Elk, S. V. Jerome, M. P. Repasky and J. C. Shelley, *J. Chem. Theory Comput.*, 2023, **19**, 2380–2388.